LAWRENCE
LIVERMORE
NATIONAL
LABORATORY

LLNL-JRNL-462672

Validation of the thermal transport model used for ITER startup scenario predictions with DIII-D experimental data.

T. A. Casper, W. H. Meyer, G. L. Jackson, T. C. Luce, A. W. Hyatt, D. A. Humphreys, F. Turco

November 18, 2010

Nuclear Fusion

Disclaimer

Validation of the thermal transport model used for ITER startup scenario predictions with DIII-D experimental data.

T.A. Casper,[1] W.H. Meyer,[1] G.L. Jackson,[2] T.C. Luce,[2] A.W. Hyatt,[2] D.A. Humphreys,[2] and F. Turco[3]

[1]Lawrence Livermore National Laboratory, Livermore, California, USA.

[1]Present address for T.A. Casper: ITER Organization, Route de Vinon sur Verdon, F-13115 St Paul lez Durance, France.

[2]General Atomics, P.O. Box 85608, San Diego, California 92186-5608 USA.

[3]Oak Ridge Associated Universities, Oak Ridge, Tennessee.

e-mail contact of main author: thomas.casper@iter.org or casper@fusion.gat.com

Abstract. Control simulations of ITER startup using 2D free-boundary equilibrium and 1D transport codes rely on accurate predictions of the electron and ion temperature profiles that determine the electrical conductivity and pressure profiles during the current rise. We present results of validation studies that apply the transport model used by the ITER team to DIII-D discharge evolution and compare predictions with data from similarity experiments. Results presented here detail difficulties and sensitivities associated with the modeling of time-dependent current profile evolution required to asses performance of the poloidal field coil system and controllers on ITER.

PACS numbers: 52.25Fi, 52.25Xz, 52.55Fa, 52.65Kj

1. Introduction

The ITER experiment [1] represents a significant advance for the world fusion energy program in both the physical size and stored energy and will be the first experiment that produces significant fusion power. With its high current capability (15 MA), a significant amount of stored energy even during the current ramp phase, and magnetic coil geometry ITER represents a challenge to the control system that must maintain both shape and vertical position. Proposed target scenarios can approach controllability limits [2,3] while loss of control may have serious consequences [4]. ITER scenarios exhibit high plasma elongation $\kappa_X \sim 1.85$ with correspondingly high vertical instability growth rates, particularly for the higher values of internal inductance, $\ell_i(3)$, that result during L-mode Ohmic startup where, for values of $\ell_i(3) > 1.1$, the vertical position becomes more difficult to control. (In this paper, we quote the $\ell_i(3)$ values for internal inductance to be consistent with definitions used in ITER publications [1,4,5]). The value of $\ell_i(3)$ is a global measure of effects related to the current density profile. The actual controllability will depend on details of the current density profile, the elongation, the controller used and system noise present.

Currently, the operational space available to ITER is being studied with a variety of equilibrium and time-dependent transport codes [6]. Based on these calculations, the ITER coil specifications, the nature of operating scenarios, and system limitations are being reviewed to evaluate engineering constraints prior to construction to resolve any operational limits as indicated by experiments currently in operation. The basis for many

of these studies is free-boundary equilibrium and transport simulations [6,7,8,9] to evaluate the operational space and the ability of the controller to maintain the shape and vertical position. Assumptions concerning the thermal transport characteristics in the ITER device must be made to perform these predictive studies.

In addition to the simulation efforts, scaled ITER-like experiments are being conducted in many existing tokamaks [10]. From these experiments, the viability of the various operating scenarios and vertical stability can be assessed. Data from these discharges is available to evaluate the code predictions for the existing experiments. This gives a basis for scaling the operational characteristics to an ITER-sized plasma. We have been conducting such experiments at the DIII-D National Fusion Facility [11] to explore startup conditions [12], demonstration discharges for operational scenarios [13], and ramp down techniques [14]. To scale the ITER device in DIII-D, we compress time by 50:1 to account for the different current diffusion time scales between the two experiments. The size is scaled by 3.5, the ratio of the major radii in the two devices. Using the flexible poloidal field coil system in DIII-D, we can closely match the plasma shape achieved in DIII-D to that proposed for ITER operational scenarios as we show in figure 1. Details of many of these DIII-D ramp up discharges have been published [12].

This work seeks to validate the transport model used for ITER predictions with simulations of DIII-D pulse evolution for different startup conditions and comparisons with the experimental discharge. The DIII-D predictive modeling is done exactly as in the ITER simulations in order to determine the fidelity of the predictions for ITER performance. In this effort, we are not adjusting parameters of the transport model to achieve the best overall fit to experimental data but rather holding model parameters

fixed as a validation of the ITER modeling process. Start up predictions are of scientific interest since all of ITER performance is determined by the ability to establish the desired current distribution, and a vertically stable ramp up is demanding for the control system. For the purpose of validation, we simulate several different start-up scenarios. These include the initial start-up scenario [8] with a small, circular plasma limited on the outside wall referred to as the "small bore start up". The relatively new "large bore" startup for ITER [10] is addressed as well. This assumes ITER will start up with a large volume plasma limited on the outside wall that has been found in experiments to be more attractive. Finally, validation of startup with different current ramp rates is done using experiments with the feedback-control of internal inductance. This modifies the current density profile during the ramp up and provides experimental validation for the different current density profiles.

2. Transport model and code

In many of the recent ITER controller performance simulation studies, a model based on gyro-Bohm scaling laws and profile consistency has been used to model the thermal transport characteristics [15]. We refer to this as the Coppi-Tang (C-T) model which was initially compared with data from the TFTR [16] experiment. This model provided reasonably good agreement with experimental data for predictions of the temperature evolution in circular-shaped plasma. In studying controller performance using free-boundary equilibrium evolution, coupling to the external circuits (poloidal coil system) is required for feedback control of shape and vertical stability. The thermal transport characteristics must be defined on the entire cross-section to get both the pressure and current density from the magnetic axis to the separatrix including the H-mode edge bootstrap current region that affects controller response. For L-mode plasmas, the C-T model is defined for the entire normalized toroidal flux coordinate, ρ, over the interval $\rho = 0. - 1.$ and provides a fast and stable model for long duration simulations of ITER scenarios [7]. These simulations start early in the current ramp (~ 3.5 s in ITER) and evolve the plasma properties during the burn (to ~ 500 s) and into the current ramp down phase (to ~ 700 s).

Details of the transport model determine the gross shape of the ion and electron temperature profiles as various heating sources provide energy input to the plasma. Thermal conductivity profiles resulting from the C-T model are determined from a toroidal-flux profile shape factor that is dependent on the profiles for heating and electron density multiplied by an exponential form factor resulting from the assumption of a

parabolic temperature profile in steady state [16]. In this sense, the model is limited in its capability of describing the radial structure of the temperature profiles. The central temperature is determined by the gyro-Bohm scaling derived from theoretical arguments with the overall transport adjusted by a scale factor representative of a scaling-law based semi-empirical model. For the model validation we are concerned with here, we consider only the L-mode phase during the current ramp up. We adjust the overall transport with a constant scale factor applied over $\rho = 0. - 1.$ to scale the energy confinement time. This scale factor was chosen to be 2.5 for several ITER simulations completed by various research groups [6] to match the 0D confinement predictions for ITER [1]. We used the same value to simulate DIII-D discharges and compare with the DIII-D temperature evolution in order to benchmark the model used for the ITER predictions.

We use the CORSICA code [17] for these studies. It is a 2D equilibrium and 1D transport predictive integrated modeling code that can operate in several modes [7] using either free-boundary or fixed-boundary solvers to simulate the discharge equilibrium evolution. For our studies here, since we are interested in validating the transport model with experimental data, we prescribe the time-dependent shape evolution so as not to introduce variations due to differences in plasma shape between simulation and experiment. In this case, we use the EFIT [18] equilibrium-fitting code to analyze the experimental data to get the shape evolution (rather than using free-boundary with a controller to determine the plasma shape). This insures that the plasma shape agrees well with the actual shape during the experiments. We determine the plasma separatrix boundary every 0.1 s in DIII-D from some desired start time after breakdown where the equilibrium is well behaved (typically by ~ 0.3 s into the discharge). As we evolve the

plasma conditions, we do a 2D-interpolation between these fiducial shapes to evolve the plasma shape with vertical stability maintained by this prescribed shape evolution.

In the transport-simulation case, the C-T transport model determines the evolution of the electron and ion temperature profiles. We use a constant electron temperature boundary condition of 20eV at the separatrix location (normalized toroidal flux = 1). The edge temperature depends upon details of complex interaction between power flow across the separatrix, ionization processes, divertor performance and wall recycling. Prediction of the boundary temperature requires full core-edge-coupled simulations that are not currently available and has only recently been considered for development. We chose not to evolve the edge temperature boundary condition so as to remain consistent with the predictive modeling being done for ITER. The value used is, however, consistent with the edge temperature measurements on DIII-D. The equilibrium solver coupled to Ohm's law evolves the internal flux state including flux diffusion and gives the resulting current-density profile. We assume resistivity is neoclassical and evaluate it using the NCLASS model [19]. To avoid modeling fueling and particle transport, we use the fitted density profile obtained from the Thomson scattering diagnostic on DIII-D. This puts the focus on temperature evolution effects. Most ITER start up experiments do not have neutral-beam heating and thus lack charge-exchange-recombination (CER) data needed for reliable impurity measurements. For these cases, we assume a fixed ratio of carbon impurity density to the measured electron density to provide a Z-effective profile consistent with other experiments on DIII-D. When the CER data is available, we use its measurement of impurity density in the modeling. Since we are concerned with how well the thermal transport model fits the experimental data, we have found it useful to use

comparative simulations with the electron temperature profile also obtained from measurements using data from the Thomson scattering instrument for spline fits of smoothed electron temperature profiles. This gives a measurement-based temperature profile reference for the calculations that use the electron temperature profile from transport to benchmark both the equilibrium and current profile evolution without the assumed thermal transport. We then compare the simulations of current profile using the fitted electron temperature profiles with those obtained using the electron temperature profiles calculated from the thermal transport model.

3. Small and large bore startup cases

We have completed validation experiments for the C-T transport model using both small- and large-bore startup scenarios. In the small-bore startup originally specified for ITER [8], small, circular plasmas are formed on the outside limiter, diverted at about 25 s for ITER, and then elongated and shaped as the current is ramped up to full value. This was the original ITER startup scenario. In the large-bore case [10], a large volume plasma is formed early in time and quickly brought to the diverted (at about 13 s) and shaped configuration. Following experiments coordinated through the International Tokamak Physics Activity, the large bore startup has been adopted as the ITER startup reference case. The ITER first wall design does not allow significant auxiliary heating while the plasma is limited. For this reason, most discharges in DIII-D simulating the ITER scenario have been done without neutral-beam heating during the current ramp. A single short-pulse (20ms duration) from the neutral-beam system is often present for diagnostic purposes, but even a single short pulse introduces a noticeable perturbation to the electron temperature evolution with respect to Ohmic heating. For this reason, we generally do not have time-dependent measurements that rely on neutral beam injection (NBI). In particular, we do not have ion temperature or impurity density profile measurements from the charge-exchange recombination (CER) diagnostic. We also lack internal constraints on the current profile from the Motional Stark Effect (MSE) [20] diagnostic and, therefore, have no measurement of the on-axis safety factor, q_0, evolution. When we lack MSE data, EFIT analysis is done either with only the magnetics data or, in the case of a kinetic EFIT, with the fitted pressure profile. The lack of MSE data leads to potential systematic errors in the experimental data analysis and in the simulations. We show in

figure 2, parameters representative of a large-bore startup scenario discharge in DIII-D. Small-bore conditions are similar except the current ramp rate and flattop current may be different. For these experiments, the toroidal field is $B_T = 2.1\,\mathrm{T}$ and flattop plasma current in the range of $I_p = 0.9 - 1.6\,\mathrm{MA}$.

In figure 3, we show the current ramp-up for shot 127990 that is typical of a small-bore startup in DIII-D along with results of validation simulations using CORSICA. CORSICA uses the (smoothed) measured total I_p to feedback control plasma current in this simulation. We did not attempt to track the I_p ramp variation from 0.5 s to 0.7 s due to the switching of the direction of solenoid power supply in the experiment [figure 3(a)]. In figure 3(b), we show a comparison of the on-axis safety factor, q_0, evolution using electron temperature profiles prescribed from the measurements and those calculated with the C-T transport model. We also show data from an electron cyclotron emission (ECE) diagnostic channel near the magnetic axis. We note that, for the evolution with the prescribed temperature, q_0 passes the $q_0 = 1$ value at the same time the ECE measurement shows the onset of large sawteeth. This indicates we have good agreement in the simulation with the experimental equilibrium and current profile evolution. When we turn on the thermal transport model, we see that the q_0 passes through unity slightly earlier than the onset of sawteeth indicating a slightly more peaked current density profile in the simulated evolution than in the experiment. In figure 3(c) we compare the internal inductance of the simulation with the fitted equilibria. We note that the CORSICA evolution with the prescribed profiles is in good agreement with the EFIT results used for profile analysis. However, when the thermal transport model is used, there is a significant

difference in the value of $\ell_i(3)$ indicating a modeling error due to errors in the conductivity profile (from the electron temperature evolution) coupling non-linearly into the evolution of the current density profile and, therefore, into the stored magnetic energy. The coupling results because the Ohmic plasma current produced by the coil system in DIII-D inductively drives current primarily at the edge of the plasma. The profile for the toroidal current density depends sensitively on the conductivity profile as determined by the electron temperature profile arising from the Ohmic heating power available. The inward flux diffusion that ultimately determines the spatially inward evolution of the current density profile depends on this conductivity. Thus, small errors in the "edge" temperature profile roughly outside a normalized toroidal flux of 0.75 can significantly alter the spatial evolution of the current density which, in turn, leads to the deviation in the internal inductance obtained.

In figure 4, we show comparisons of the electron temperature profiles obtained from transport with the spline-fitted profiles from measurements. We observe that the gross agreement is generally quite good. Between $t = 0.5$ s and 0.6 s, there is a short pulse from the NBI system [figure 3(a)] and the experiment clearly responded more strongly to this pulse of input energy than did the simulation. A general trend, however, is that the edge T_e profile from transport is lower than measured profiles and this feature significantly affects the equilibrium evolution and results in the modeling error observed for ℓ_i. While there are small differences in the T_e profiles near the magnetic axis, they do not significantly alter the core current profile evolution and result in only a small error in the time of sawtooth onset.

We define the prediction error between the measured and predicted electron temperature profiles as $E(\rho,t) = T_{em}(\rho,t) - T_{ep}(\rho,t)$ from which we calculate the root-mean-square error by averaging the square of the error minus its mean value over either time or toroidal flux. The total flux-averaged error for each of the profiles is shown in figure 4 (rms$E$). This is an average over flux of the prediction error at each time and provides a measure of the relative quality of the prediction from the C-T model. We also define a normalized error as $E_n(\rho,t) = E(\rho,t)/T_{ep}(\rho,t)$. In figure 5, we show the time-averaged root-mean-square errors for both the prediction and normalized prediction errors calculated as the sample averages over time at each value of toroidal flux. We observe the average prediction error is relatively small and lowest near the separatrix. However, the average normalized prediction error rises significantly in the edge region and this modeling error drives the rise in $\ell_i(3)$ as the temporal evolution of the conductivity affects the current density profile evolution.

These observations are quite consistent over a range of experimental simulations. The transport model does a reasonably good job of predicting the temperature profile and the overall core current profile as evidenced by q_0 evolution. However, it tends to show an offset in $\ell_i(3)$ that sets in early in the simulation as the edge temperature profile adjusts. In figure 6, we show comparison of both large- and small-bore startup validation simulations. In these two cases, we have taken the measured electron temperature profile, the measured electron density profile, and assumed $T_i = 0.9\ T_e$ based on the limited ion temperature data available. Variations in the multiplier down to $0.5\ T_e$ indicate the results are not sensitive to the exact value assumed. These quantities were used to calculate the experimental pressure profile. We use this in the EFIT analysis to constrain the pressure

as we do in the CORSICA case without transport. We find very good agreement between the prescribed-profile EFIT results and those from CORSICA indicating that, if the T_e is accurately known, the solutions to the equilibrium subject to neoclassical resistivity do an excellent job in predicting the experimental evolution. However, the modeling results again show $\ell_i(3)$ to move rapidly away from the prescribed profile result early in time. Again, this is due to relatively small errors in the temperature profile evolution nonlinearly coupling into the current profile evolution. In figure 6(d), we also show a simulation using the transport model where we have increased the boundary temperature (T_e at $\rho = 1$) from 0.02 to 0.05 keV to demonstrate the sensitivity to the edge temperature profile in predicting $\ell_i(3)$. The experimental profiles show much more variation in the shape of T_e at the edge than do those obtained from the C-T model. Basically the C-T model edge T_e profile from $\rho = 0.7$ to 1 changes little over the time interval from 0.4 s to 0.6 s and this is the root cause of the $\ell_i(3)$ difference.

We note that the difference between the simulated and data-reconstructed $\ell_i(3)$ tends to be larger for the large-bore startup case than for small-bore conditions. Even though there is an offset in ℓ_i, the evolution tends to capture the time-variations quite well. In the large-bore case [figures 6(c) and (d)] where the simulation tracks the plasma current ramp-up variation more accurately, we observe the transient affect on the $\ell_i(3)$, from $t = 1.1$ to 1.2 s. In both cases, we finally note that after the NBI power comes on [$t = 0.85$ s in figure 6(a) and $t = 1.6$ s in figure 6(c)] and NBI heating dominates the Ohmic power, the error in the $\ell_i(3)$ is reduced. With the onset of H-mode conditions due to NBI heating, the edge bootstrap current dominates $\ell_i(3)$ and the $\ell_i(3)$ is reduced with

the larger off-axis current density resulting from the formation of the H-mode edge barrier.

4. Feedback control on $\ell_i(3)$ cases

During our experimental investigation of ITER startup options, we developed the capability for feedback control of $\ell_i(3)$ in order to vary $\ell_i(3)$ using the plasma current ramp rate [12]. In these experiments, we used multiple NBI pulses for diagnostic measurements during the current ramp up. In our validation simulations for these $\ell_i(3)$-feedback experiments, we use the exact measured I_p versus time to control the simulation plasma current (rather than implement the feedback algorithm in CORSICA at this time). We show two large-bore feedback current ramp-up cases in figure 7 (note the factor of 2 difference in time scales plotted). The case shown in figure 7(a) has a higher current ramp rate producing the lower $\ell_i(3)$ as is shown in figure 8 discussed later, since the flux diffuses inwards more slowly with respect to the rate of change in plasma current. The current profile remains less peaked during the ramp until it is fully diffused late in time. In these discharges, since we used several NBI pulses, we now have the data needed to evaluate current-constrained EFIT fitted equilibria using the MSE diagnostic [20] data and do not resort to the kinetic analysis of EFIT. We observe that there is good agreement between the temporal evolution of q_0 for the MSE-EFIT analysis of experimental data and the transport profile result from CORSICA. Again, there is good agreement between the onset of sawtooth fluctuations observed on the ECE diagnostic with the time that $q_0 \sim 1$.

In figure 8 we show the evolution of $\ell_i(3)$ for these two large-bore startup cases. We see the effect of the modeling error on the $\ell_i(3)$ evolution. This tends to be larger for the higher current ramp rate case [figures 8(a) and 8(b)]. Again we have included the

simulation with the higher edge T_e of 0.05 keV for shot 132500 [figure 8(d)] to indicate the sensitivity to edge temperature assumptions in the simulation. We also note that we again recover the time-dependent characteristics of the $\ell_i(3)$ evolution when compared with the EFIT results. In figure 9, we show the temperature profiles for discharge 132500 [figures 8(c) and 8(d)]. As in the earlier small-bore startup case, we have generally good agreement between the T_e from transport and those from the Thomson diagnostic measurements. The differences in the shape of the T_e profile near the magnetic axis results in a slightly more peaked core current-density profile and the earlier time for q_0 to reach unity. The small errors in the edge Te profile again result in errors in the $\ell_i(3)$ evolution when compared with the EFIT fitted equilibrium results. As shown in figure 5(b), the overall prediction error is low over the entire radius but the normalized error is large near the edge region and again drives this difference between the measured and predicted electron temperature profiles and the rise in the $\ell_i(3)$ through the resistivity affecting the evolution of the toroidal current density profile

5. Summary

We have completed several experiments on the DIII-D tokamak to simulate the ITER current ramp-up using the scaled ITER shape. We use spatial and temporal scaling to translate the DIII-D shape and current evolution to that expected in ITER. We have done simulations of these DIII-D discharges to benchmark the predicted evolution of the temperature profile and thus the resistivity and current profile evolution anticipated in ITER. We use the C-T transport model with parameters identical to those used in several ITER scenario performance and controller simulations that predict the potential performance of the ITER device and used to explore various engineering limitations of the controller and coil system. In these validation studies, we find that, as quantified in the error analysis in figure 5, the C-T transport model does a reasonably good job in predicting the gross structure of the electron temperature profile evolution.

However, differences in the details of the electron temperature profile evolution when compared with the measurement on DIII-D lead to significant errors in evolution of the current density profile in approximately the outer quarter of the plasma due to deviations in the edge temperature prediction. We note that the time of onset of sawtooth fluctuations as evidenced by the time q_0 falls below unity tends to be a little earlier with the C-T transport temperature profiles than expected from the fitted equilibrium and the saw-tooth fluctuations observed on the ECE diagnostic near the magnetic axis. This indicates the simulation with the electron temperature from the C-T transport model yields a somewhat more peaked current density profile earlier in time, e.g. a more rapid flux diffusion in the simulations than present in the experiment. Perhaps more importantly, we note that the C-T-model tends to underestimate the edge electron

temperature (outside $\rho \sim 0.75$) when compared with the measured profiles. This results in a current profile evolution with a lower current-density profile near the edge and thus a higher $\ell_i(3)$ early in time. When evaluating the nature of a transport model, it is not sufficient to merely evaluate the model under steady conditions but rather one must explore the time-varying effects on the plasma properties. For the ITER predictions, the higher ℓ_i, if present, would give rise to a greater demand on the poloidal field set to supply flux necessary for controlling the vertical position. If the $\ell_i(3)$ for ITER would indeed be lower than the predictions of the model used, then the vertical control during ramp up would likely be less demanding on the controller.

These simulations are intended to benchmark the transport model as it has recently been applied to study ITER performance and controllability. We have not attempted to tune the transport model to get better agreement with the experimental data. Instead, our desire was to benchmark the transport model and hence the predictions being made for ITER performance. Indeed, our experiments and simulations indicate that caution needs to be exercised when interpreting the many predictive studies [6,7,8,9] of ITER performance. This work suggests that significant care must be taken in using transport models to generate performance specifications for ITER.

Acknowledgment

This work has been performed under the auspices of the U.S. Department of Energy under Contracts DE-AC52-07NA27344 and DE-FC02-04ER54698.

References

[1] M. Shimada *et al* Progress in the ITER Physics Basis Chapter 1: Overview and summary 2007 Nucl. Fusion **47** S1-S17

[2] D.A. Humphreys *et al* in Fusion Energy 2008 (Proc. 22nd Int. Conf. Geneva, 2008) (Vienna: IAEA) CD-ROM file 2-4Rb and http://www-naweb.iaea.org/napc/physics/FEC/FEC2008/html/index.htm

[3] A. Portone *et al* in Fusion Energy 2008 (Proc. 22nd Int. Conf. Geneva, 2008) (Vienna: IAEA) CD-ROM file 2-4Ra and http://www-naweb.iaea.org/napc/physics/FEC/FEC2008/html/index.htm

[4] Y. Gribov *et al* Progress in the ITER Physics Basis Chapter 8: Plasma operation and control 2007 Nucl. Fusion **47** S385-403

[5] D.J. Ward *et al* Nucl. Fusion **33** (1993) p821.

[6] C.E. Kessel *et al* Nucl. Fusion **49** (2009) 085034.

[7] T.A. Casper *et al* 2008 Fus. Eng. Design **83** 552-556

[8] A. Loarte *et al* Progress in the ITER Physics Basis Chapter 4: Power and particle control 2007 Nucl. Fusion **47** S203-S263

[9] S-H. Kim *et al*, Plasma Phys. Control. Fusion **51** (2009) 105007.

[10] A.C.C Sips *et al* Nucl. Fusion **49** (2009) 085015.

[11] M.R. Wade *et al* 2007 Nucl. Fusion **47** S543-S562

[12] G.L. Jackson *et al.*, Nucl. Fusion **48** (2008) 125002

[13] E.J. Doyle *et al.* in Fusion Energy 2008 (Proc. 22nd Int. Conf. Geneva, 2008) (Vienna :IAEA) CD-ROM file EX/1-3 and http://www-naweb.iaea.org/napc/physics/FEC/FEC2008/html/index.htm

[14] P.A. Politzer et al Nucl. Fusion **50** (2010) 035011

[15] W.M. Tang 1986 Nucl. Fusion **26** 1605

[16] S.C. Jardin *et al* 1993 Nucl. Fusion **33** 371

[17] J.A. Crotinger *et al* LLNL Report UCRL-ID-126284, 1997 available from NTIS #PB2005-102154

[18] L.L. Lao *et al* Nucl. Fusion **30** (1985)1611

[19] W.A. Houlberg *et al* 1997 Phys. Plasmas **4** 3230

[20] C.T. Holcomb *et al* 2006 Rev. Sci. Instrum. **77** 1

Figure Captions

Figure 1. Comparison of a fully-diverted ITER shape with that achieved using the DIII-D poloidal-field coil system. The ITER shape, coils, and passive structure have been scaled approximately by the ratio of major radii. The scaled coils show the difference in the geometry and flexibility between the ITER and DIII-D coil systems.

Figure 2. Plasma parameters of a typical large-bore startup discharge, 133176: (a) Plasma current (I_p) and neutral-beam injection power (P_{inj}), (b) edge safety factor (q_{95}) and internal inductance $\ell_i(3)$, (c) electron density (n_e) on-axis from Thomson data fits, (d) electron temperature (T_e) on-axis from Thomson data fits and an ECE channel near the magnetic axis, (e) ion temperature (T_i) from CER diagnostics after neutral beams are turned on and normalized pressure (β_N) and (f) visible light data (D_α) from a view of the centerpost (inner limiting surface).

Figure 3. Shot 127990, small-bore startup discharge: (a) plasma current from experimental measurements and CORSICA simulation and neutral beam injection power, (b) ECE T_e measurement channel near the magnetic axis and q_0 evolution from CORSICA simulations with prescribed and C-T transport T_e profiles, (c) $\ell_i(3)$ evolution for EFIT profile analysis and CORSICA with T_e profiles from the measurements and the C-T transport model. The arrow indicates the error in the magnetic stored energy introduced by modeling the electron temperature evolution. (d) Comparison of measured loop voltage with that required to sustain Ohmic current in CORSICA where the difference is due to edge plasma resistivity.

Figure 4. Small-bore discharge electron temperature profiles at selected times during the current ramp up from fitted Thomson scattering measurements and the C-T transport

model in the CORSICA simulation. The profile times are shown along with the total rms error (rms$E$ - keV) averaged over toroidal flux for the profile shown.

Figure 5. Root-mean-square errors averaged over time for (a) shot 127880 averaged from 0.2 to 0.8s and (b) shot 132500 averaged from 0.4 to 3.0s for the total error (dashed, units of keV) and total normalized error (solid, dimensionless). The larger error at the edge indicates that it is the error in electron temperature between the C-T transport and measured profiles that drives the difference in $\ell_i(3)$ evolution.

Figure 6. Small-bore (127987) and large-bore (133176) startup discharges: The plasma current from experimental measurements and CORSICA simulation and the neutral-beam injection power are shown in (a) and (c) for the two discharges. The $\ell_i(3)$ evolution is shown in (b) and (d) for the kinetic EFIT analysis and CORSICA simulations with fitted and C-T-transport T_e profiles using a 0.02 keV T_e boundary condition. Also shown in (d) is $\ell_i(3)$ for the C-T-transport T_e profiles with a 0.05 keV boundary condition. The arrow indicates the error in the stored magnetic energy introduced by the transport modeling.

Figure 7. Large-bore ramp-up discharges from the $\ell_i(3)$-feedback experiments with 132411 the fast current ramp and 132500 the slow current ramp: (a,d) plasma current from measurements and the CORSICA simulation and neutral beam injection power, (b,e) ECE T_e measurement channel near the magnetic axis with onset of sawteeth at $t \sim 1$ s, T_e^{axis} from Thomson data fits and T_e^{axis} from C-T transport model simulation using CORSICA, and (c,f) q_0 evolution for MSE-constrained EFIT analysis and C-T-transport T_e profiles from the simulation. Note that the plot time scales for the two cases shown are different by approximately a factor of 2.

Figure 8. Large-bore ramp-up discharges from $\ell_i(3)$-feedback experiments: (a,d) plasma current ramp where the I_p-ramp from (a) is shown in (d, dashed) and (b,e) $l_i(3)$-control

set point and $\ell_i(3)$ evolution from real-time EFIT analysis in the controller, MSE-constrained EFIT analysis and CORSICA C-T transport simulation with 0.02 keV boundary temperature. Also shown in (e) is the C-T transport case with 0.05 keV boundary temperature. The arrow indicates the transport modeling error. Note that the plot time scales for the two cases shown are different by approximately a factor of 2. (c,f) Comparison of measured loop voltage with that required to sustain the Ohmic current in CORSICA where the difference due to edge plasma resistivity.

Figure 9. Large-bore discharge electron temperature profiles at selected times in the current ramp up for fitted Thomson profile analysis and the C-T transport model simulation in CORSICA. The profile times are shown along with the total rms error $(\mathrm{rms}E - \mathrm{keV})$ averaged over toroidal flux for the profile shown.

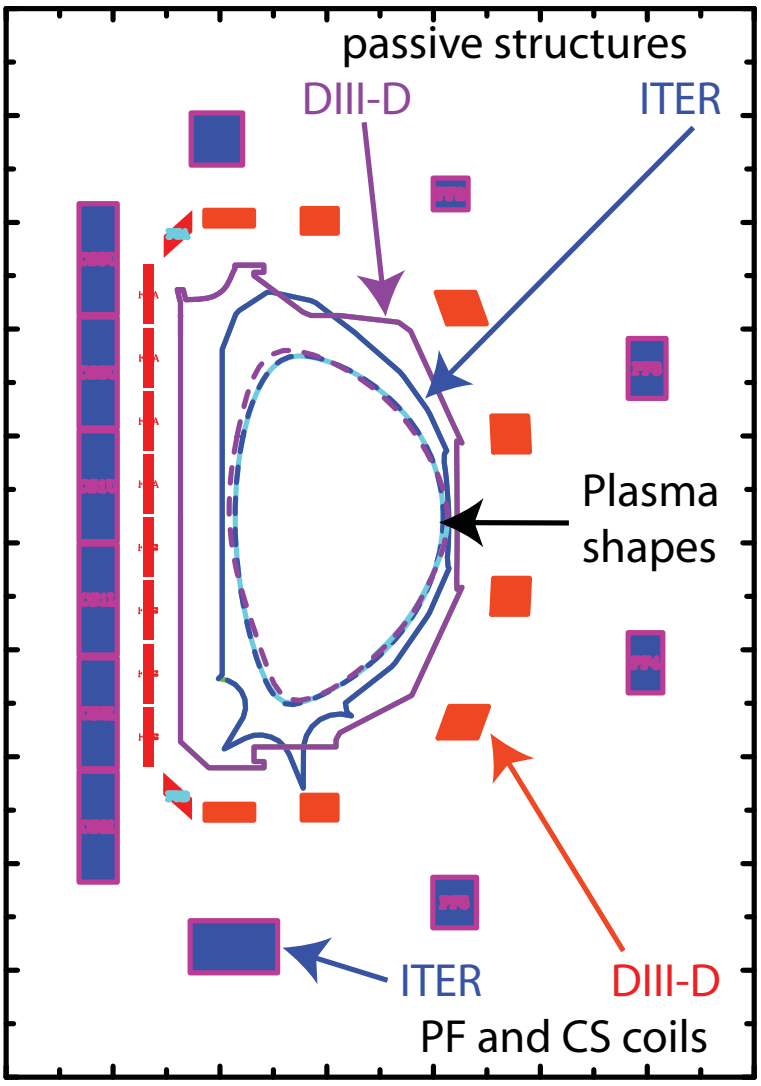

T.A. Casper, Figure 1

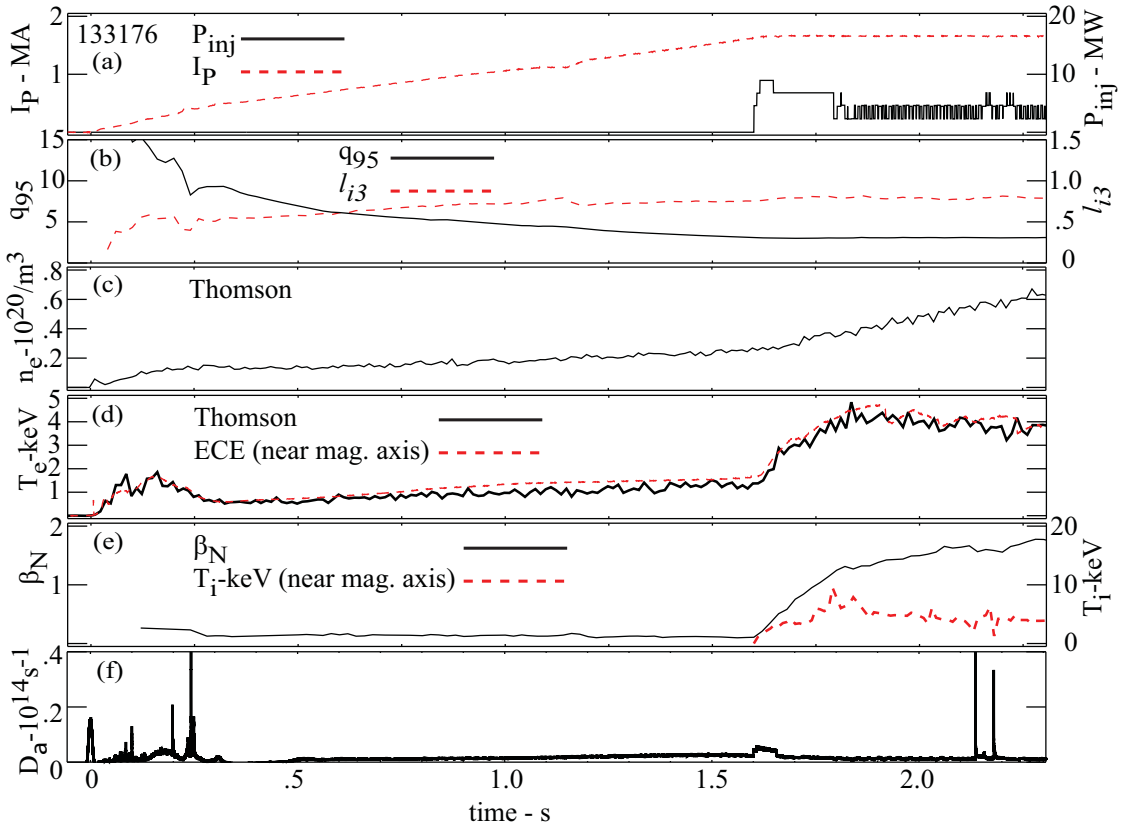

T. A. Casper, Figure 2

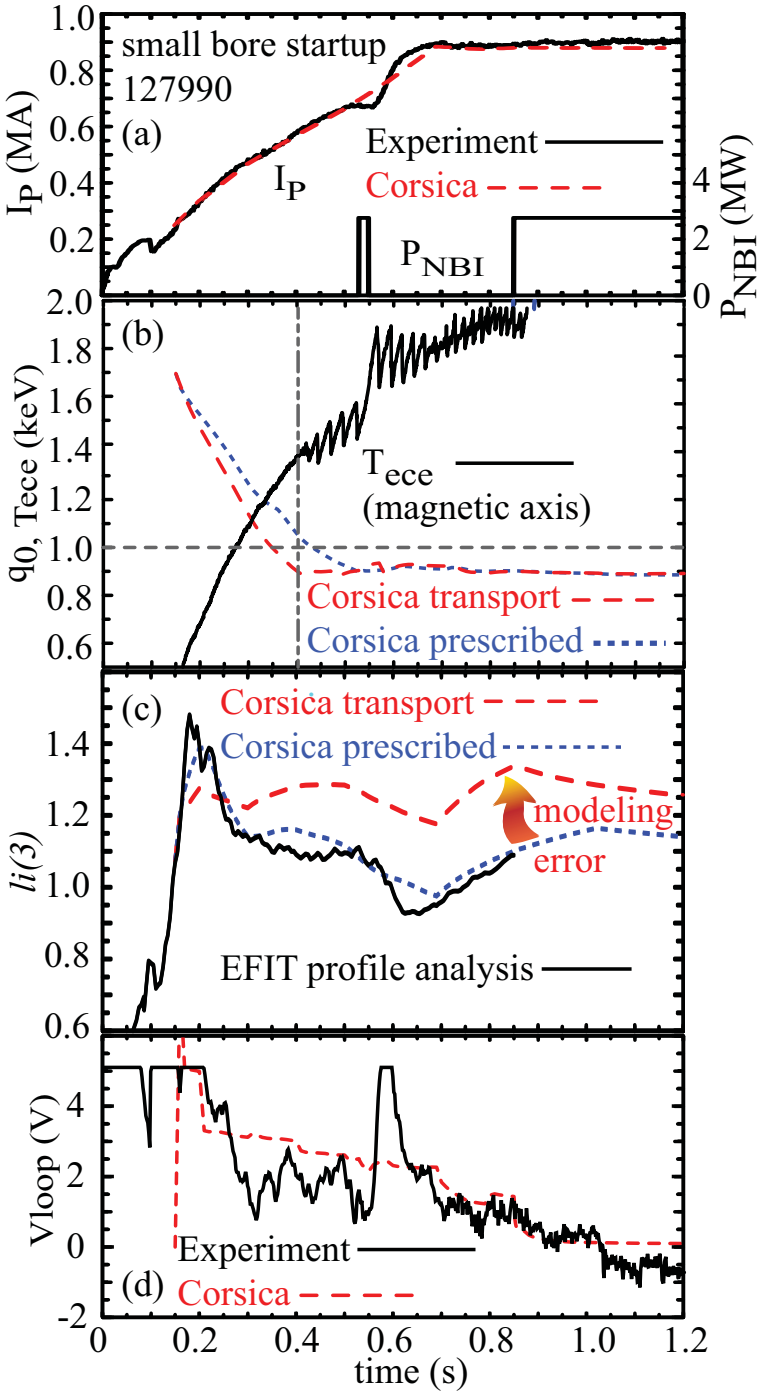

T. A. Casper, Figure 3.

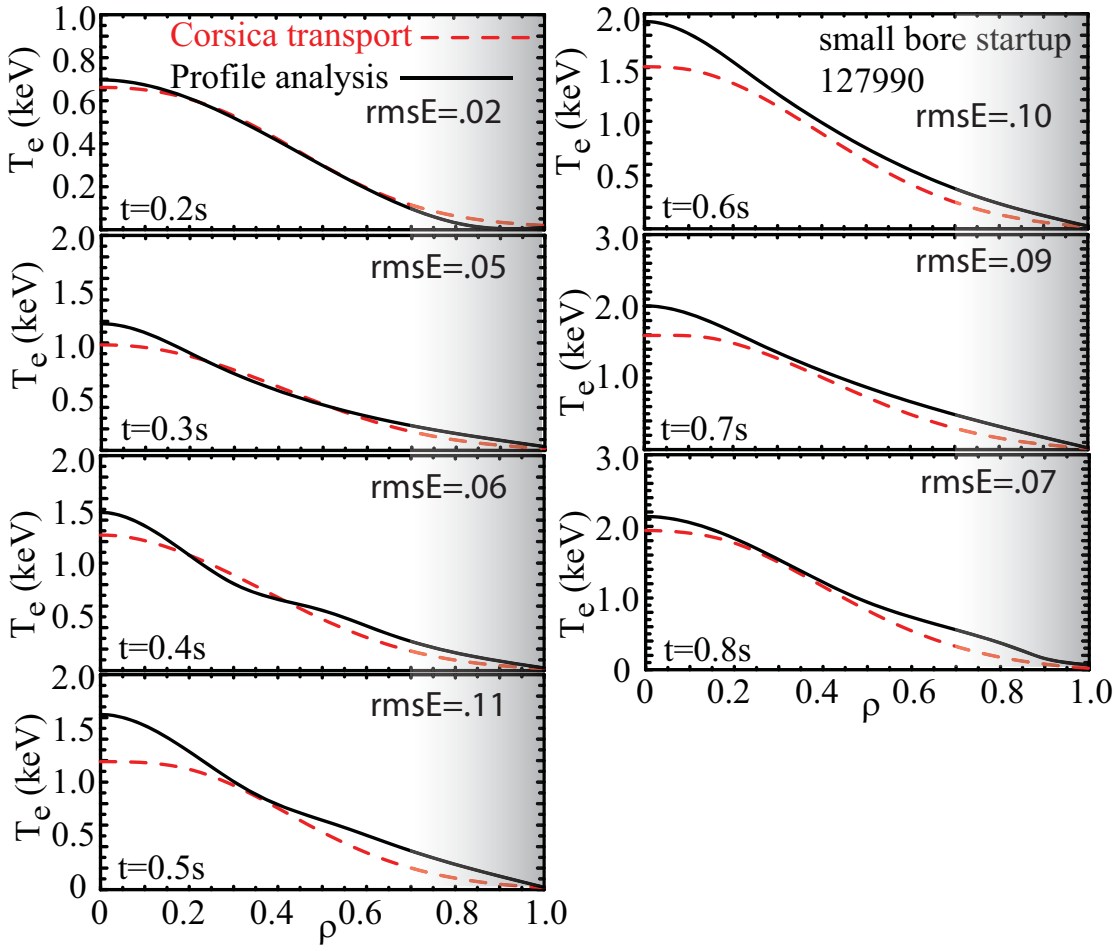

T.A. Casper Figure 4.

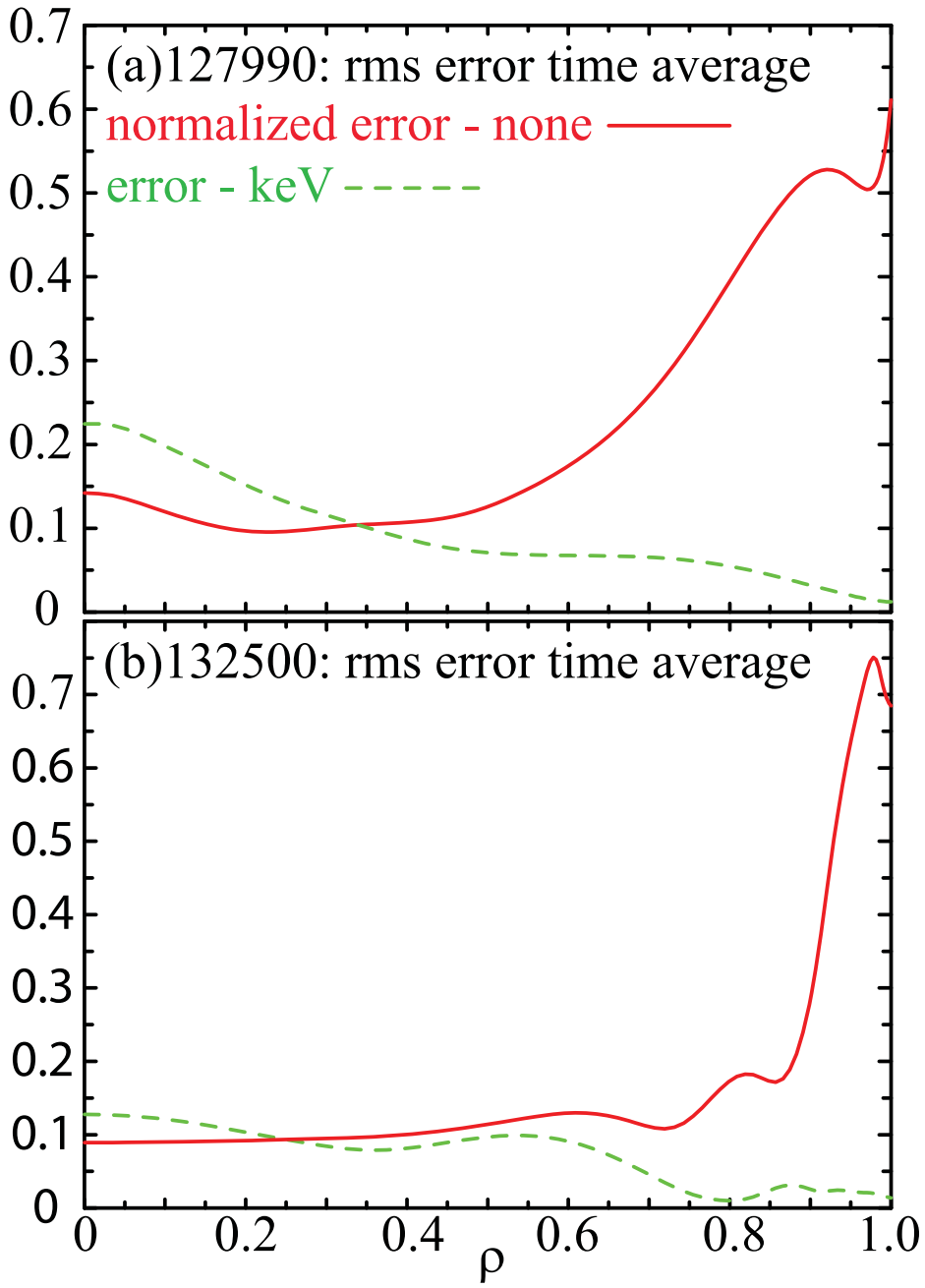

T.A. Casper Figure 5.

T.A. Casper Figure 6

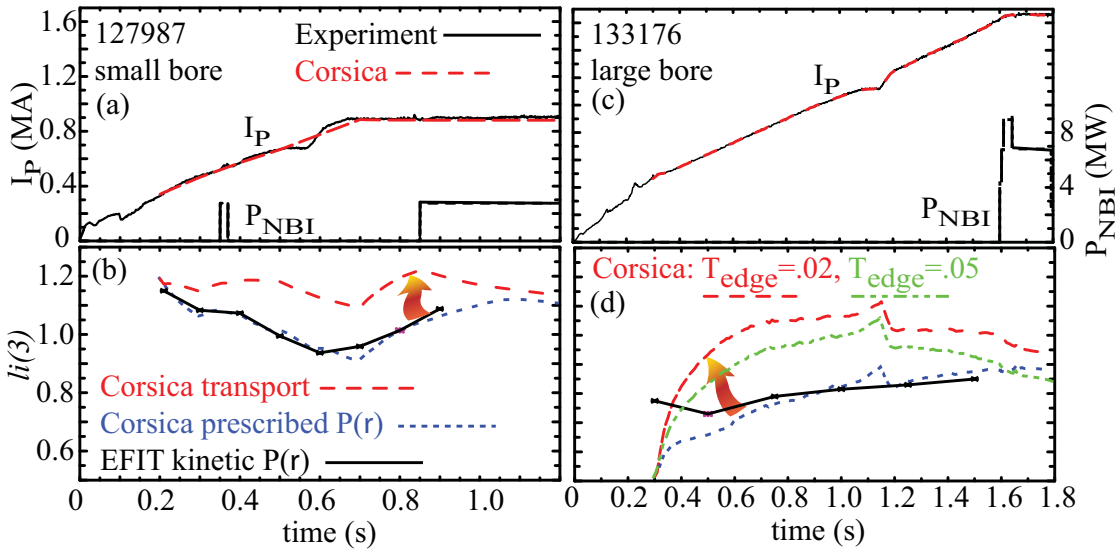

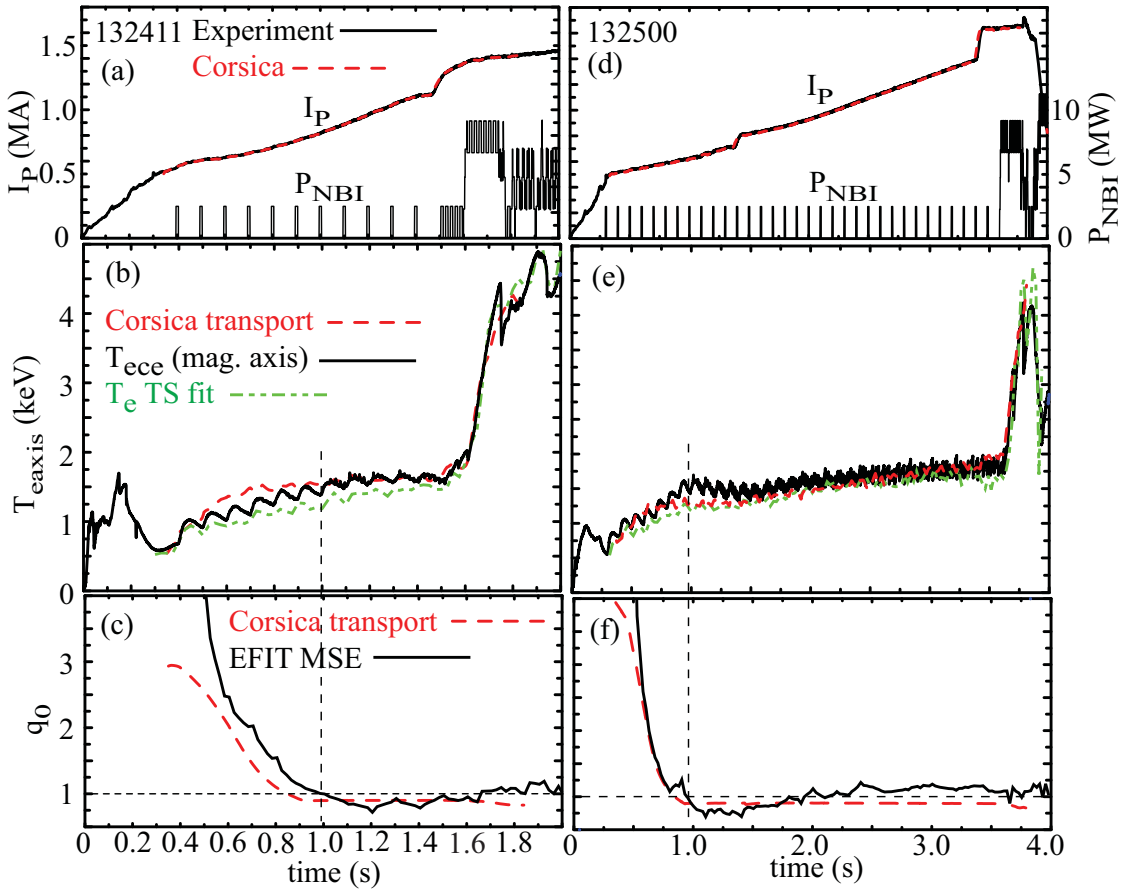

T.A. Casper Figure 7

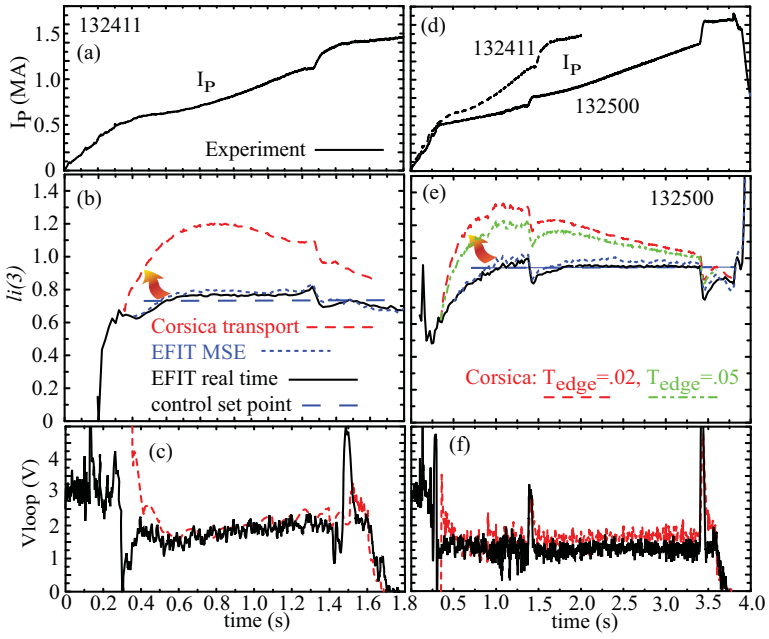

T.A. Casper Figure 8

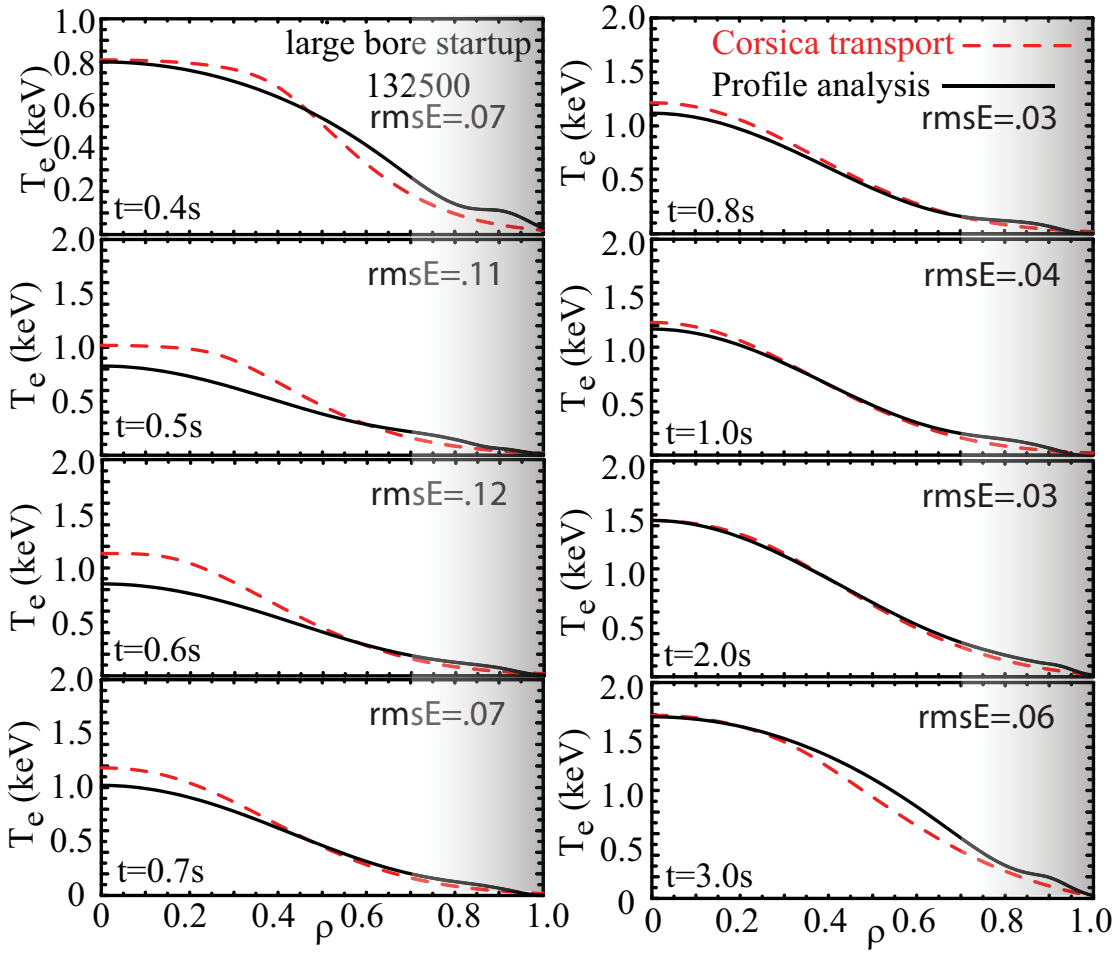

T.A. Casper Figure 9